

**Please cite the Published Version**

Mullan, DJ, Barr, ID, Flood, RP, Galloway, JM, Newton, AMW and Swindles, GT (2021) Examining the viability of the world's busiest winter road to climate change using a process-based lake model. *Bulletin of the American Meteorological Society*, 102 (7). E1464-E1480. ISSN 0003-0007

**DOI:** <https://doi.org/10.1175/bams-d-20-0168.1>

**Publisher:** American Meteorological Society

**Version:** Accepted Version

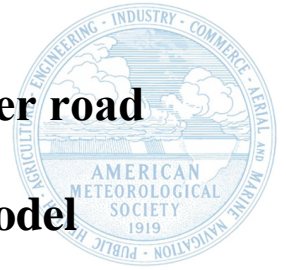
**Downloaded from:** <https://e-space.mmu.ac.uk/627482/>

**Usage rights:** © In Copyright

**Additional Information:** Copyright 2021 American Meteorological Society (AMS).

**Enquiries:**

If you have questions about this document, contact [openresearch@mmu.ac.uk](mailto:openresearch@mmu.ac.uk). Please include the URL of the record in e-space. If you believe that your, or a third party's rights have been compromised through this document please see our Take Down policy (available from <https://www.mmu.ac.uk/library/using-the-library/policies-and-guidelines>)



# Examining the viability of the world's busiest winter road to climate change using a process-based lake model

\*D.J. Mullan<sup>1</sup>, I.D. Barr<sup>2</sup>, R.P. Flood<sup>1</sup>, J.M. Galloway<sup>3</sup>, A.M.W. Newton<sup>1</sup>, G.T. Swindles<sup>1,4</sup>

<sup>1</sup>Geography, School of Natural and Built Environment, Queen's University Belfast, Belfast,  
Northern Ireland, UK

<sup>2</sup>Department of Natural Science, Manchester Metropolitan University, Manchester, UK

<sup>3</sup>Geological Survey of Canada, Calgary, Alberta, Canada

<sup>4</sup>Ottawa-Carleton Geoscience Centre and Department of Earth Sciences, Carleton University,  
Ottawa, Ontario, Canada

\*Corresponding Author Email: [D.Mullan@qub.ac.uk](mailto:D.Mullan@qub.ac.uk)

## Abstract

Winter roads play a vital role in linking communities and building economies in the northern high latitudes. With these regions warming two to three times faster than the global average, climate change threatens the long-term viability of these important seasonal transport routes. We examine how climate change will impact the world's busiest heavy-haul winter road – the Tibbitt to Contwoyto Winter Road (TCWR) in northern Canada. The FLake freshwater lake model is used to project ice thickness for a lake at the start of the TCWR – first using observational climate data, and second using modelled future climate scenarios corresponding to varying rates of warming ranging from 1.5°C to 4°C above preindustrial temperatures. Our results suggest that 2°C warming could be a tipping point for the viability of the TCWR, requiring at best costly adaptation and at worst alternative forms of transportation. Containing

**Early Online Release:** This preliminary version has been accepted for publication in *Bulletin of the American Meteorological Society*, may be fully cited, and has been assigned DOI 10.1175/BAMS-D-20-0168.1. The final typeset copyedited article will replace the EOR at the above DOI when it is published.

25 warming to the more ambitious temperature target of 1.5°C pledged at the 2016 Paris  
26 Agreement may be the only way to keep the TCWR viable – albeit with a shortened annual  
27 operational season relative to present. More widely, we show that higher regional winter  
28 warming across much of the rest of Arctic North America threatens the long-term viability of  
29 winter roads at a continental scale. This underlines the importance of continued global efforts  
30 to curb greenhouse gas emissions to avoid many long-term and irreversible impacts of climate  
31 change.

32

### 33 **Capsule**

34 Warming of 2°C may be a tipping point for the world’s busiest winter road, while enhanced  
35 winter warming threatens the viability of winter roads across Arctic North America.

36

### 37 **Introduction**

38 The Arctic has experienced warming two to three times greater than the long-term global mean  
39 trend of 0.87°C since preindustrial times (IPCC 2018), resulting in widespread shrinking of the  
40 cryosphere (IPCC 2019). This arctic amplification is projected to continue throughout the 21<sup>st</sup>  
41 century, with a 2°C global mean temperature increase (GMTI) projected to result in up to a  
42 6°C warming in the Arctic (IPCC 2018). While impacts on ice sheets and glaciers tend to  
43 capture the headlines, there are also important consequences for infrastructure in Arctic and  
44 sub-Arctic communities, where warming temperatures threaten the physical integrity of  
45 overland transport routes and the economies they sustain (Meredith et al. 2019). Infrastructure  
46 built over permafrost is particularly vulnerable. Cumulative expenses of USD 5.5 billion are  
47 projected for climate-driven damage to public infrastructure in Alaska between 2015 and 2099  
48 under high emissions scenarios, with one of the top two costs associated with building damage  
49 from near-surface permafrost thaw (Melvin et al. 2017). In a circumpolar study, Hjort et al.

50 (2018) revealed that nearly four million people and 70% of existing infrastructure in the  
51 permafrost domain lie in areas with high potential for near-surface permafrost thaw. Winter  
52 roads, comprising seasonally frozen sea, land, lakes, rivers, and creeks, are also under  
53 considerable threat from a warming climate. These seasonal roads are vital for the affordable  
54 transport of heavy equipment, cargo and fuel, but also provide physical connections that foster  
55 social and cultural interactions among remote communities (Chiotti and Lavender 2008; Furgal  
56 and Prowse 2008). In recent decades, climate change has shortened the operational season of  
57 winter roads across the Canadian Arctic, and published studies project future shortening in the  
58 James Bay region of Ontario (Hori et al. 2016; 2018); northern Manitoba and Saskatchewan  
59 (CIER 2006; Blair and Sauchyn 2010); the Mackenzie River, Northwest Territories (ACIA  
60 2005); and the Tibbitt to Contwoyto Winter Road, Northwest Territories (Perrin et al. 2015;  
61 Mullan et al. 2017). One commonality in the methods used in these previous studies is that  
62 future projections are based on regression models developed between historic climate trends  
63 and ice thickness records. While there is merit in this statistical approach, it lacks a process-  
64 based incorporation of the multitude of meteorological and lake-specific parameters that  
65 influence the development of lake ice (Dibike et al. 2012). Given this limitation, the present  
66 study applies – for the first time – a process-based freshwater lake model to simulate the  
67 impacts of climate change on winter roads. We do this by examining the future viability of the  
68 world’s busiest heavy-haul winter road to GMTIs of 1.5°C, 2°C and 4°C above preindustrial  
69 temperatures. We also make inferences for the future viability of other winter roads across  
70 Arctic North America based on projected winter warming in the region.

71

## 72 **Study Region, Materials and Methods**

73 The study region is the Tibbitt to Contwoyto Winter Road (TCWR), Canada – a seasonally  
74 operational winter road extending from Tibbitt Lake, Northwest Territories ~ 70 km east of

75 Yellowknife and spanning around 400 km northwards across frozen lakes (85%) and overland  
76 portages (15%) to Ekati diamond mine, north of Lac de Gras (JVTC 2020) (Figure 1). The  
77 TCWR is of considerable economic importance as the only overland transport route supplying  
78 four mines with fuel, cement, tyres, explosives, and other construction and maintenance  
79 materials to a value of CAD 500 million yr<sup>-1</sup> (JVMC 2015). It is the busiest heavy-haul winter  
80 road in the world, with more than 300,000 tonnes transported in over 10,000 loads yr<sup>-1</sup> (Perrin  
81 et al. 2015). This annual haulage has, on average, been squeezed into a shorter transport season  
82 (herein referred to as the operational season) over the past twenty years, at least in part driven  
83 by rising air temperatures in the region (Appendix Figure A1).

84

### 85 *A modelling approach*

86 We simulate ice thickness for Tibbitt Lake (62.56°N, 113.36°W) at the southern limit of the  
87 TCWR using the FLake freshwater lake model (<http://www.flake.igb-berlin.de/site/download>)  
88 (Kirillin et al. 2011). FLake simulates the vertical temperature structure and mixing conditions  
89 of shallow lakes ( $\leq 50$  m) (Huang et al, 2019). It is used as a lake parameterisation module in  
90 three-dimensional numerical weather prediction and climate models, but can also run in stand-  
91 alone mode as a single-column lake model (Mironov 2008). We apply FLake in stand-alone  
92 mode, simulating ice thickness for 20-year simulations at a daily time step representing (1)  
93 observed climate, and (2) a set of 15 future climate scenarios. We applied the model on a  
94 hydrological year basis – with each year beginning on 1 October and ending on 30 September.  
95 This approach is employed to ensure model simulations begin prior to the annual onset of ice  
96 freeze up.

97

### 98 *Simulations under observed climate*

99 FLake first requires a set of lake-specific parameters. Lake depth (6.7 m) was taken from Crann  
100 et al. (2015) and fetch (2000 m) was approximated by maximum lake length, measured using  
101 Google Earth™. The extinction coefficient ( $0.6 \text{ m}^{-1}$ ) for water transparency was estimated from  
102 field notes associated with Galloway et al. (2010) – a number representing clear water. For a  
103  $0.5^\circ \times 0.5^\circ$  grid square containing Tibbitt Lake, daily mean temperatures, relative humidity,  
104 solar radiation, and wind speed data from 1 October 1985 – 30 September 2005 were taken  
105 from the Watch Forcing Dataset Era Interim (WFDEI) (Weedon et al. 2014), accessed through  
106 the Earth System Grid Federation (ESGF) (<https://esgf-node.llnl.gov/>). Cloud cover data were  
107 unavailable from WFDEI and instead taken from the European Centre for Medium-Range  
108 Weather Forecasts (ECMWF) next-generation reanalysis (ERA5) (C3S 2017), accessed  
109 through the Copernicus Climate Data Store (CDS) (<https://cds.climate.copernicus.eu/>) for a  
110  $0.5^\circ \times 0.5^\circ$  grid square containing Tibbitt Lake. The October 1985 – September 2005 time  
111 period was chosen for two reasons: (1) the observational data are required to bias correct future  
112 climate scenarios in a later step based on its comparison to a model hindcast period, with most  
113 model hindcast periods ending in 2005; and (2) 1986-2005 is the historical baseline period used  
114 by the Intergovernmental Panel on Climate Change (IPCC) in their Fifth Assessment Report  
115 (AR5) (IPCC 2013). FLake was run under the observed climate, with dates recorded when lake  
116 ice thickness exceeded 107 cm (the safe minimum limit for heavy-haul vehicles) (Perrin et al.  
117 2015). Since there are no measured ice thickness data for Tibbitt Lake, we compared measured  
118 records for four analagous shallow sub-arctic Canadian lakes (locations shown in Figure 1)  
119 with FLake simulations for the same lakes. The measured data were taken from Environment  
120 and Climate Change Canada (Environment and Climate Change Canada, 2020) and were  
121 available for a minimum of 10 years between 1981 and 2000, with FLake simulations run for  
122 the same years following an identical approach to input data as described above for Tibbitt  
123 Lake. Validation results indicate the model has a tendency to underestimate ice thickness early

124 and late in the lake ice season, while observed ice thickness in the heart of the lake ice season  
125 is generally overestimated (Appendix Text A1, Figure A2).

126

### 127 *Simulations under future climate*

128 FLake was then run under a series of future climate scenarios corresponding to GMTIs of  
129 1.5°C, 2°C and 4°C. The former two rates of warming reflect pledges made by 195 countries  
130 under the 2016 Paris Agreement (UNFCCC 2015) and are therefore considered mitigation  
131 scenarios, whereas the latter represents something approximating a no-mitigation scenario – a  
132 rate of warming evaluated as being *as likely as not* to be exceeded by the end of the 21<sup>st</sup> century  
133 under the highest representative concentration pathway (RCP) 8.5 (IPCC 2013). To account  
134 for arctic amplification we examined how the selected GMTIs corresponded to warming in the  
135 study region and found that 1.5°C, 2°C and 4°C equated to 2.9°C, 3.9°C and 7.8°C (Appendix  
136 Text A2). These are herein referred to as regional mean temperature increases (RMTIs). For  
137 each RMTI, we shortlisted five climate scenarios (n=15) from an initial pool of 82 available,  
138 based on how closely they compared to observations at a monthly temporal resolution for a  
139 hindcast period from 1986-2005 (Appendix Text A3, Table A1). Daily mean temperatures from  
140 the 15 model scenarios were then downloaded from the ESGF and CDS for the grid square  
141 containing Tibbitt Lake. All scenarios are part of the Coupled Model Intercomparison Project  
142 (CMIP5) (Taylor et al. 2012), forced with RCP8.5 (van Vuuren et al. 2011) – a high radiative  
143 forcing scenario necessary to capture RMTIs up to 7.8°C. For each scenario, we extracted the  
144 20-year future time period when projected temperatures reached 2.9°C, 3.9°C and 7.8°C above  
145 preindustrial temperatures. Projected temperatures were bias corrected using the change factor  
146 methodology used in Ho et al. (2012) (Appendix Text A4). Only temperatures were modified  
147 from the baseline FLake simulations, with the other meteorological parameters left constant.  
148 This reflects the dominant role that air temperatures play in changing lake ice conditions

149 (Brown and Duguay 2010), but also the fact that some of the other meteorological parameters  
150 are unavailable from many of the selected climate models. FLake was then run under each  
151 projected climate scenario and the dates recorded when lake ice thickness exceeded the 107 cm  
152 threshold. The projected operational season of the TCWR for each model was adjusted to  
153 reflect the difference between the baseline simulations and the historical operational season of  
154 the TCWR (JVTC 2020) (Appendix Text A5). We also downloaded temperatures for the period  
155 1 October 2000 – 31 September 2020 from ERA5 (C3S 2017) to capture years post-2005 and  
156 allow us to relate these to the TCWR operational season observations. Present and future  
157 operational season length was then colour coded in a traffic light system based on an economic  
158 analysis conducted by Perrin et al. (2015). Green indicates  $\geq 50$  days – a viable season; amber  
159 indicates 45-49 days – an ‘adaptive scenario’ where flexible scheduling is required to meet  
160 season demands at a high cost of around USD 1.57 million yr<sup>-1</sup>; and red indicates < 45 days –  
161 a ‘critical conditions scenario’ representative of an unviable season and the need for alternative  
162 transportation at a cost of around USD 6.09 million yr<sup>-1</sup>.

163

#### 164 *Providing wider geographical context*

165 In order to set our results for the TCWR within a wider geographical context, we downloaded  
166 monthly observed temperatures from ERA5 (C3S 2017) and monthly CMIP5 climate model  
167 scenarios for each of the 15 future scenarios used in the FLake simulations for the northern half  
168 of North America (40°N – 90°N, 55° – 180°W). Future scenarios were interpolated to the same  
169 resolution as the observed data and then bias corrected using a change factor approach, by  
170 subtracting the hindcast period of the model from the future period and adding the result to  
171 observations (Hawkins et al. 2013).

172

#### 173 **Results and Discussion**



174 Projected changes in the TCWR operational season relative to the present are shown in Figure  
175 2. The mean length of the operational season is projected to decrease for all but one of the 15  
176 future scenarios, from 61 days at present to 56-61 days under 1.5°C, 47-55 days under 2°C and  
177 20-31 days under 4°C. The range reflects differences in climate model scenarios. Although not  
178 directly comparable because we focus on rates of warming rather than set time periods, changes  
179 are broadly in line with previous projections for the TCWR. Perrin et al. (2015) projected a  
180 mean operational season of 58 days by the 2020s and 49 days by the 2050s, while a much  
181 shorter operational season of 21, 5 and 2 days was projected by Mullan et al. (2017) for the  
182 2020s, 2050s and 2080s respectively. The particularly extreme scenarios in the latter may  
183 reflect limitations in the regression modelling methodology, lending support to the process-  
184 based lake modelling conducted here. According to the Perrin et al. (2015) classification, our  
185 results suggest that warming of 1.5°C permits a viable TCWR operational season, but an  
186 increase to 2°C leads to costly adaptation under two scenarios. A warming of 4°C shows a  
187 mean operational season well below the unviable threshold, indicating no future for the TCWR  
188 before this level of warming is reached. These findings suggest that, for an average year, an  
189 increase from 1.5°C to 2°C is the tipping point at which costly adaptation is required. An  
190 increase from 1.5°C to 2°C GMTI was also found to impose higher risks for a number of other  
191 natural and human systems, including in some cases long-lasting or irreversible impacts such  
192 as the loss of some ecosystems (IPCC 2018).

193

#### 194 ***Enhanced December warming and impacts on late opening***

195 From the present mean operational season of 31 January to 1 April, future changes in the mean  
196 operational season length translates to 30 January-3 February to 29-31 March under 1.5°C, 4-  
197 10 February to 26-30 March under 2°C and 18-27 February to 17-20 March under 4°C (Figure  
198 2). These dates reveal there is a general trend towards a larger proportion of the change coming

199 from a delayed opening – particularly at 4°C – with a slower rate of change in an earlier closure.  
200 Jensen et al. (2007) found a similar pattern across 65 water bodies in the Great Lakes region  
201 between Minnesota and New York, USA – with lake freeze up occurring 3.3 days decade<sup>-1</sup>  
202 later and lake breakup occurring at a slower rate of 2.1 days decade<sup>-1</sup> earlier from 1975-2004.  
203 Figure 3 explains the trend towards a greater proportion of change from a delayed opening in  
204 this study, with November-January temperatures projected to warm at a rate far in excess of  
205 February-April temperatures. For example, under a GMTI of 4°C, December temperatures in  
206 the Tibbit Lake region are projected to warm by 11.5°C compared to a 6.1°C rise in March.  
207 Temperatures in the autumn months generally act as the dominant control on lake and river ice  
208 freeze up, with reduced autumn cooling known to prolong the period of above zero water  
209 temperatures and delay the onset of freeze up (Prowse et al. 2007). Hori et al. (2018) refer to  
210 these months, primarily October-December in the high latitudes, as the preconditioning period  
211 of winter roads – essential for providing a more climatically favourable construction period  
212 and contributing to earlier opening dates. When warming of the magnitude projected here  
213 occurs during this preconditioning period, it is unsurprising that a considerable delay in the  
214 opening of the TCWR follows. Figure 3 reveals this pattern could be expected to an even larger  
215 degree across much of the rest of Arctic North America, with a GMTI of 1.5°C, 2°C and 4°C  
216 resulting in regional December warming in excess of 5°C, 8°C and 15°C across parts of the  
217 Prudhoe Bay coast of Alaska, the Northwest Territories, Nunavut, and the Hudson Bay coastal  
218 regions of Manitoba, Ontario and Quebec. With a number of prominent winter roads in these  
219 regions, a widespread shift towards costly adaptation or route closure seems likely.

220

221 The levels of winter warming projected here – in places over three times the global average –  
222 are consistent with projections for the Arctic by the end of the 21<sup>st</sup> century (IPCC 2013; 2019).  
223 These high rates of warming can be explained by a projected continuation of arctic

224 amplification, where observed records in recent decades show a warming signal that has been  
225 strongest over the Arctic Ocean in autumn and winter (Cohen et al. 2014; Horton et al. 2015).  
226 A number of mechanisms are thought to be responsible for enhanced sensitivity to warming in  
227 the Arctic, but chief among them is the change in sea ice albedo owing to the stark difference  
228 in reflective properties of an ice-free ocean and snow-covered sea ice surfaces (*ca.* 7% vs 80%  
229 reflectance respectively) (Cohen et al. 2019). This likely explains the high degree of warming  
230 particularly along the Arctic coastal regions in autumn and winter (Figure 3). Other more  
231 localised arctic amplification mechanisms may contribute to enhanced autumn and winter  
232 warming in the study region, located ~ 500 km south of the Arctic coast. Local forcings include  
233 snow, cloud and ice insulation feedbacks (Kwok et al. 2009; Lee et al. 2011; Yang and  
234 Magnusdottir 2018), while increased vegetation over Arctic land contributes to surface  
235 darkening at high latitudes (Overland et al. 2015). It is thought that local and remote forcing  
236 mechanisms may interact and amplify one another (Yang and Magnusdottir 2018), meaning  
237 some combination of all the above factors is likely at play in amplifying warming in the wider  
238 TCWR region. Attribution studies indicate that increasing anthropogenic greenhouse gases  
239 play a vital role in driving Arctic surface temperature increases (Fyfe et al. 2013; Najafi et al.  
240 2015), leading to a high confidence in projections of further Arctic warming (Overland et al.  
241 2018).

242

### 243 *Interannual variability*

244 The interannual variability within the 20-year observations and simulation periods reveals that  
245 mean patterns are subject to considerable divergence from year to year, as shown in Figure 4.  
246 During the observed period, the TCWR opened as late as 9 February in 2016 (9 days later than  
247 the mean), while it closed as early as 21 March in 2010 (11 days earlier than the mean). As  
248 seen in Figure 4 and in Figure A1, shortened seasons are often associated with anomalously

249 warm years, partly due to large-scale teleconnections that correlate most strongly with  
250 Canadian climate during winter (Bonsal and Shabbar 2011). Anomalous heating in the Eastern  
251 tropical Pacific associated with El Niño results in a positive Pacific-North American (PNA)  
252 pattern over North America (Wallace and Gutzler 1981) and consequently warmer than average  
253 temperatures from late autumn to early spring (Shabbar and Khandekar 1996). The two shortest  
254 operational seasons on record (2010: 46 days; and 2016: 44 days) follow two of the strongest  
255 El Niño events in recent decades: 2009/10 and 2015/16 (Timmermann et al. 2018). Shorter  
256 operational seasons in some cases may also be associated with increased winter storminess.  
257 Major storms with high wind speeds and blowing snow can cause temporary closures on the  
258 road, as occurred in March 2012 (Rodan 2012). Where anomalously warm or stormy winters  
259 cause the ice to break open in a ‘blowout’ (Ashbury 2006), winter roads may shut for  
260 maintenance or may even close for the season. The short 50-day season in 2006 occurred in  
261 such a way, with a blowout on Waite Lake late in the season (14 March) before the season was  
262 complete (Perrin et al. 2015). Consequently, approximately 1,200 loads were flown into mines  
263 in the summer and autumn of 2006 at a cost of CAD 100-150 million (JVMC 2014; Perrin et  
264 al. 2015). A poleward shift in extratropical cyclone activity is projected to result in increased  
265 atmospheric moisture and greater winter precipitation over the northern half of North America  
266 (Christensen et al. 2013). This indicates the clear future potential for an increase in blowing  
267 snow and hazardous blizzards that further threaten the operational season of the TCWR.  
268 Conversely, longer operational seasons are typically associated with colder than average years.  
269 For example, the longest operational season on record (26 January – 16 April 2002: 81 days)  
270 occurred when 2001/02 winter and early 2002 spring temperatures were considerably colder  
271 than average. Cooler years are typically associated with modes of variability in opposite phases  
272 to anomalously warm years. A switch towards La Niña events and a negative phase of the PNA  
273 are associated with earlier freeze up and later breakup of lake and river ice across much of

274 Canada (Bonsal et al. 2006). Figure 4 shows that interannual variability in temperatures and  
275 the winter road operational season are projected to continue in future, indicating that natural  
276 variability will continue to result in considerable year to year divergence from the mean. Figure  
277 2 shows that the year with the longest projected operational season under 1.5°C (69-79 days)  
278 and 2°C (63-72 days) is always longer than the mean observed season (61 days) and reflective  
279 of a viable season in the Perrin et al. (2015) classification. In addition, Figure 2 shows that the  
280 mean projected operational season is always longer at 1.5°C (56-61 days) and 2°C (47-55 days)  
281 than it is during the shortest year of the observed record (44 days). Figure 5 reveals the reason  
282 for this, as temperature anomalies during the warmest observed year are higher than the mean  
283 temperature anomalies for 1.5°C and 2°C for all months under most future scenarios (note this  
284 refers to the warmest observed year out of 20 simulated years, where the actual year may differ  
285 between months). Furthermore, the year with the longest projected operational season at 4°C  
286 (37-50 days) is for two models greater than the shortest observed operational season (44 days).  
287 Figure 5 again shows why, since the year with coldest projected temperatures under 4°C is  
288 colder than the warmest observed year during January-April. In this sense, greater future  
289 variability may offer hope that colder than average years could permit some fully operational  
290 seasons, even when the mean suggests otherwise. For example, under the least extreme 2°C  
291 model – where a mean operational season of 55 days is projected – there are 12 years out of 20  
292 where a fully viable season up to the longest year of 72 days is projected.

293

294 However, greater future variability also means there are several years that fall below the mean.  
295 The same 2°C scenario referred to above has a shortest season length of 36 days and eight out  
296 of 20 years that fall below the 50-day threshold. Considering the shortened 50-day season and  
297 associated high costs in 2006, it is clear that scenarios such as the one identified above do not  
298 lend support to a viable TCWR without at least considerable adaptation. Even under 1.5°C

299 scenarios, where the mean operational seasons of all five models exceed the 50-day threshold,  
300 shortest seasons lie below 40 days – with several years among the 20-year projections falling  
301 below the viable threshold. For example, under the least extreme 1.5°C model – where the  
302 mean season length is 61 days – there are still four years out of 20 where the operational season  
303 is less than 50 days. Falling short of a viable season length at a frequency of once every five  
304 years may raise important questions among planners about the long-term viability of the  
305 TCWR. That outlook becomes even bleaker when we examine the most extreme 1.5°C and  
306 2°C scenarios, with seven out of 20 years below the 50-day threshold for the former, and 11  
307 years for the latter. At 4°C, the TCWR is unequivocally unviable. Three out of five models  
308 under the 4°C scenarios project all 20 years to fall below the 50-day threshold, with the other  
309 two models projecting only one or two years respectively above this threshold. As shown in  
310 Figure 5, temperatures rising above freezing in November and April under these scenarios  
311 indicates why such large reductions in the operational season are simulated.

312

### 313 *Adaptation*

314 Before considering costly large-scale adaptation options, there are first adaptations to present-  
315 day practices that may help ensure the TCWR remains viable for longer. Sladen et al. (2020)  
316 investigated threshold requirements for the initiation of winter road operations along the  
317 TCWR and found that the current practice of planning construction by calendar dates rather  
318 than by evaluation of air-freezing indices results in a conservative approach to the start of the  
319 construction season. In the interests of ‘winning back’ some time as the climate reduces the  
320 length of the operational season, it may be necessary to adapt a more methods-based approach  
321 to the dates of winter road construction, by installing equipment to calculate freezing indices  
322 or measure frozen ground depths and temperatures. It is also clear, however, that such an  
323 approach incurs expense, logistical challenges and issues with mobilising equipment and

324 personnel at short notice (Sladen et al. 2020). Amending the nature of annual haulage on the  
325 TCWR may also represent a low-cost adaptation measure in the face of shortening operational  
326 seasons. For winter roads linking remote communities, the desire is to ensure as long a season  
327 as possible. This is not the case for the TCWR, where the goal is to ensure specified tonnages  
328 of materials to mines are provided during the operational season. Where the season length is  
329 reduced, lost service may be recovered by increasing the number of daily loads (Perrin et al.  
330 2015). We see evidence of this in the historical records (Appendix Table A2) – years with a  
331 reduced operational season but higher freight statistics than years with a longer season. For  
332 example, 2016 ranks third out of 20 years for highest number of loads (8,766) and tonnes  
333 transported (262,261), despite being the shortest operational year (44 days) on record. This  
334 clearly shows there is some scheduling flexibility that can help offset a shortened operational  
335 season. The limiting factor in this scenario is the number of trucks and drivers available (Perrin  
336 et al. 2015). Increasing their provision to facilitate maximising the daily use of the TCWR may  
337 therefore avoid more costly adaptation. The above adaptations may help under the less extreme  
338 scenarios highlighted in this study, but larger-scale higher-cost alternatives may be needed  
339 under more extreme scenarios. Options already considered for the TCWR include construction  
340 of an all-season gravel-surface overland route along the most vulnerable southern portion;  
341 construction of a deep sea port at Bathurst Inlet, Nunavut, with a road to the mines across colder  
342 Arctic tundra; and construction of 600 km of power lines to expand hydroelectric power and  
343 reduce reliance of the mines on diesel – the most transported commodity in the TCWR (Perrin  
344 et al. 2015). If pledges to reduce greenhouse gas emissions are not met, there may be little  
345 alternative but to implement one or more of these measures to protect economic activity in the  
346 region.

347

## 348 **Conclusions, Limitations and Future Work**

349 Unlike previous studies, use of a process-based freshwater lake model has allowed us to  
350 incorporate more of the factors influencing the development and evolution of lake ice along  
351 the TCWR. Despite this, there are a number of limitations that must be considered when  
352 interpreting the results. FLake has been found to overestimate ice thickness (e.g. Kheyrollah  
353 Pour et al., 2012) – a trend clearly evident in our validation (Figure A2) during the peak cold  
354 season between January and March. We also identified an underestimation of ice thickness in  
355 November/December and in April/May, corresponding with slightly later than observed  
356 freezeup (by 3 days on average) and earlier breakup (by 9 days on average). These  
357 freezeup/breakup trends are similar to some studies (e.g. Kheyrollah Pour et al., 2012; Rontu  
358 et al., 2019) and opposite in sign to others (e.g. Yang et al., 2013; Kourzeneva, 2014;  
359 Peitikäinen et al., 2018). Timing of overestimation and underestimation in our validation results  
360 likely points to difficulties in simulating the accumulation of snow on lake ice (Rontu et al.,  
361 2019). FLake does not account for the insulating effect of snow, meaning ice is able to thicken  
362 more rapidly but also melt faster without snow buffering ice from the cold air above (Jeffries  
363 and Morris, 2006). Although provision is made to model parametrically the evolution of snow  
364 cover above lake ice in FLake, the model has not been sufficiently tested in this regard and is  
365 highlighted as an area requiring development (FLake, 2020). It is not possible to quantify in  
366 days the potential impact this limitation has on the operational season length of the TCWR, but  
367 we highlight this as a particular point of caution when interpreting the projected dates shown  
368 in Figure 2. The daily time step may be too temporally coarse to take account of important  
369 processes relating to ice formation, including low wind speeds and calm events creating the  
370 potential for complete lake freeze within hours (Bernhardt et al., 2011). This highlights another  
371 important issue – only air temperatures were modified in the future simulations owing to data  
372 availability. This limits the reliability of future projections since interactions with other  
373 changing meteorological properties including wind speed are essential components in ensuring



374 vertical heat transfer is sufficient to cool surface water temperatures to 0°C (Leppäranta, 2010;  
375 Nõges and Nõges, 2014). Perturbing other meteorological variables in the model in addition to  
376 mean temperatures would build a fuller picture of the impacts of climate change on the TCWR.  
377 No ice thickness measurements were available for Tibbitt Lake, so it is not possible to fully  
378 evaluate model performance for the lake simulated in this study. Future studies could also build  
379 on our progress by accounting for the ~ 15% of the TCWR route crossing overland portages,  
380 which primarily comprise permafrost peatlands (Sladen et al. 2020). With rapid thawing of  
381 permafrost peatlands in the Canadian Arctic (Swindles et al. 2015; Sim et al. 2019), it is  
382 currently unclear if these sections of the TCWR are more or less vulnerable to warming than  
383 lakes. Finally, a continental or hemispheric-scale study simulating the impacts of climate  
384 change on other winter roads across the high latitudes, beyond the inferences we have made,  
385 would be highly valuable. In the meantime, our work represents a considerable advance on  
386 previous studies and highlights the escalating threat that climate change poses to the future  
387 viability of the TCWR and most likely other North American winter roads. The identification  
388 of a tipping point at 2°C GMTI illustrates that the actions of current and future generations in  
389 cutting greenhouse gas emissions is critical to the future viability of winter roads and the vital  
390 role they provide in building economies and linking communities in the northern high latitudes.

391

### 392 **Acknowledgments**

393 The authors acknowledge helpful feedback received on the manuscript from Steve Grasby,  
394 Geological Survey of Canada.

395

### 396 **Data Availability Statement**

397 References to the datasets used in this study and the web addresses for the data repositories  
398 they were downloaded from can be found in the Datasets, Materials and Methods sections (and  
399 in Appendix Text A1 and A2). All data are freely and openly available.

400

## 401 **Appendix Text**

402

### 403 **Text A1. FLake Model Validation**

404 Ice thickness data for four lakes in Canada were downloaded from Environment and Climate  
405 Change Canada. We selected the four lakes following a careful screening process that started  
406 by examining all available lake ice records from Environment and Climate Change Canada and  
407 including those lakes that fulfilled the following criteria: (1) latitude  $> 52.5^\circ$  (to ensure lakes  
408 are within  $10^\circ$  of the study lake); (2)  $> 10$  years of data between 1981-2000 (to correspond with  
409 the modelling time period for the study lake); and (3) lakes with a mean depth  $< 50$  m (as  
410 determined from the Global Lake Database) – note 50 m depth is considered the upper limit of  
411 suitability for FLake modelling. This generated a validation database comprising four lakes –  
412 the details of which are provided in Figure A2. Measurements for these four lakes exist at  
413 approximately a weekly temporal resolution and were measured to the nearest centimetre using  
414 a special auger kit or hot wire ice thickness gauge (Environment Canada, 2020). FLake  
415 simulations were run from 1 October 1981 – 30 September 2000 and were then compared to  
416 the observed ice thickness records by extracting modelled ice thickness only for the precise  
417 dates where measured data existed during the 19-year comparison period. The two sets of data  
418 were then compared for the (inclusive) months November-May, with the absolute error, mean  
419 absolute error and percentage error calculated to determine the degree to which the model under  
420 or overestimated ice thickness during these months (Figure A2). We also downloaded observed  
421 freezeup and breakup dates for each validation lake from the Global Lake and River Ice

422 Phenology Database Version 1 (Benson et al., 2020) and compared these records with FLake  
423 simulated freezeup and breakup dates for the same years as the data used to calculate absolute  
424 error (Figure A2).

425

### 426 **Text A2. Calculating RMTIs**

427 To calculate RMTIs for the study area, monthly mean temperatures were downloaded from  
428 KNMI Climate Explorer (<https://climexp.knmi.nl/>). Historical monthly mean temperatures for  
429 the period 1986-2005 were subtracted from the 2006-2100 period forced with RCP8.5 for the  
430 mean of all CMIP5 models and ensembles. This was done for the global average (resulting in  
431 2.0°C) and subsequently for the grid square containing Tibbitt Lake (resulting in 3.9°C). This  
432 global : regional ratio of 2.0 : 3.9 was subsequently used to correct GMTIs of 1.5°C, 2°C and  
433 4°C by simply dividing 3.9 by 2.0 and multiplying by the relevant GMTI. This produced  
434 RMTIs of 2.9°C 3.9°C and 7.8°C. We deducted 0.6 from each RMTI to reflect the fact that the  
435 1986-2005 period was 0.6°C warmer than preindustrial temperatures, and then calculated the  
436 mean 20-year period when temperatures were 2.3°C, 3.3°C and 7.2°C higher than the 1986-  
437 2005 hindcast period for each model.

438

### 439 **Text A3. Shortlisting climate models**

440 We downloaded all available CMIP5 models and ensembles at a monthly temporal resolution  
441 under RCP8.5 (n=82) for the grid square containing Tibbitt Lake. For all 82 scenarios, we  
442 calculated the root mean squared error (RMSE) from the difference between the 1986-2005  
443 historical temperatures for that scenario and the 1986-2005 observed temperatures for Tibbitt  
444 Lake. The 82 scenarios were ranked by their RMSE and the top five for each GMTI shortlisted  
445 for subsequent FLake modelling. In several cases, a different 20 year future time period from

446 the same scenario was used among the final 15 scenarios. The full list of selected scenarios and  
447 extracted time periods is given in Table A1.

448

#### 449 **Text A4. Bias Correction**

450 Daily temperature projections for each scenario were bias corrected using a change factor (CF)  
451 methodology that uses observed daily variability and changes the mean and daily variance as  
452 simulated by the model (e.g. Arnell et al. 2003, Gosling et al. 2009). Outlined in Ho et al (2012),  
453 this method takes the form:

454

$$455 \quad T_{CF}(t) = \overline{T_{RAW}} + \frac{\sigma T_{RAW}}{\sigma T_{REF}} (O_{REF}(t) - \overline{T_{REF}})$$

456

457 Where  $T_{RAW}$  represents daily raw model output for the future period,  $T_{REF}$  represents daily raw  
458 model output for the historical period,  $O_{REF}$  represents daily observed output, time (t) represents  
459 a daily time step, the bar above a symbol denotes the mean, and  $\sigma$  represents standard deviation.

460

#### 461 **Text A5. Operational Season Adjustment**

462 Projected operational season dates were adjusted using the following equation:

463

$$464 \quad D_{AdjOBS} = \left( \frac{D_{REF}}{D_{OBS}} \right) (D_{FUT} - D_{OBS})$$

465

466 Where  $D_{AdjOBS}$  represents adjusted projected operational season dates,  $D_{REF}$  represents  
467 projected operational dates for the baseline simulations,  $D_{OBS}$  represents operational dates from  
468 historical records (2001-2020), and  $D_{FUT}$  represents projected operational dates from future  
469 simulations.

470

471 **References**

472 ACIA, 2005: Arctic climate impact assessment. Cambridge University Press, Cambridge.

473 Arnell, N. W., D. A. Hudson, and R. G. Jones, 2003: Climate change scenarios from a regional  
474 climate model: estimating change in runoff in southern Africa. *J. Geophys. Res.*, **108**, 4519-  
475 4535, <https://doi.org/10.1029/2002JD002782>.

476 Ashbury, D., 2006: Over the top. Rio Tinto Review, No. 79: 9–14.

477 Benson, B., J. Magnuson, and S. Sharma, 2020: Global Lake and River Ice Phenology  
478 Database, Version 1. Boulder, Colorado USA. NSIDC: National Snow and Ice Data Center.  
479 Accessed 20 March 2021, <https://doi.org/10.7265/N5W66HP8>.

480 Bernhardt, J., C. Engelhardt, G. Kirillin, and J. Matschullat, 2012: Lake ice phenology in  
481 Berlin-Brandenburg from 1947-2007: observations and model hindcasts. *Clim. Change*,  
482 **112**, 791-817, DOI 10.1007/s10584-011-0248-9.

483 Blair, D., and D. Sauchyn, 2010: Winter roads in Manitoba, In: Sauchyn, D., H. Diaz, S.  
484 Kulshreshtha (Eds.) The new normal: the Canadian prairies in a changing climate. CPRC  
485 Press, Regina, pp. 322-325.

486 Bonsal, B. R., T. D. Prowse, C. R. Duguay, and M. P. Lacroix, 2006: Impacts of large-scale  
487 teleconnections on freshwater-ice break/freeze-up dates over Canada. *J. Hydrol.*, **330**, 340-  
488 353, <https://doi.org/10.1016/j.jhydrol.2006.03.022>.

489 Bonsal, B., and A. Shabbar, 2011: Large-scale climate oscillations influencing Canada, 1900-  
490 2008. Canadian Biodiversity: Ecosystem Status and Trends 2010. Technical Thematic  
491 Report No. 4. Canadian Councils of Resource Ministers, Ottawa, ON. Accessed 19 May  
492 2020, [https://biodivcanada.chm-cbd.net/sites/biodivcanada/files/2018-  
493 02/974No.4\\_Climate%20Oscillations%20April%202011\\_E.pdf](https://biodivcanada.chm-cbd.net/sites/biodivcanada/files/2018-02/974No.4_Climate%20Oscillations%20April%202011_E.pdf).

494 Brown, L. C., and C. R. Duguay, 2010: The response and role of ice cover in lake-climate  
495 interactions. *Prog. Phys. Geog.*, **34** (5), 671-704,  
496 <https://doi.org/10.1177/0309133310375653>.

497 Chiotti, Q., and B. Lavender, 2008: Ontario, In: Lemmen, D. S., F. J. Warren, J. Lacroix, E.  
498 Bush (Eds.) From impacts to adaptation: Canada in a changing climate 2007. Government  
499 of Canada, Ottawa, pp. 227-274.

500 Christensen, J. H., and Coauthors, 2013: Climate Phenomena and their Relevance for Future  
501 Regional Climate Change. In: Climate Change 2013: The Physical Science Basis.  
502 Contribution of Working Group I to the Fifth Assessment Report of the Intergovernmental  
503 Panel on Climate Change [Stocker, T.F., and Coauthors (eds.)]. Cambridge University  
504 Press, Cambridge, United Kingdom and New York, NY, USA.

505 CIER, 2006: Climate change impacts on ice, winter roads, access trails, and Manitoba First  
506 Nations. Accessed 16 June 2012,  
507 [http://www.nrcan.gc.ca/earthsciences/projdb/pdf/187b\\_e.pdf](http://www.nrcan.gc.ca/earthsciences/projdb/pdf/187b_e.pdf).

508 Cohen, J., and Coauthors, 2019: Divergent consensus on arctic amplification influence on  
509 midlatitude severe winter weather. *Nature*, **10**, 20-29, [https://doi.org/10.1038/s41558-019-](https://doi.org/10.1038/s41558-019-0662-y)  
510 [0662-y](https://doi.org/10.1038/s41558-019-0662-y).

511 Cohen, J., and Coauthors, 2014: Recent arctic amplification and extreme mid-latitude weather.  
512 *Nat. Geosci.*, **7**, 627-637, <https://doi.org/10.1038/ngeo2234>.

513 Copernicus Climate Change Service (C3S), 2017: ERA5: Fifth generation of ECMWF  
514 atmospheric reanalyses of the global climate. Copernicus Climate Change Service Climate  
515 Data Store (CDS), Accessed 19 May 2020,  
516 <https://cds.climate.copernicus.eu/cdsapp#!/home>.

517 Crann, C. A., R. T. Patterson, A. L. Macumber, J. M. Galloway, H. M. Roe, M. Blaauw, G. T.  
518 Swindles, and H. Falck, 2015: Sediment accumulation rates in subarctic lakes: Insights into  
519 age-depth modeling from 22 dated lake records from the Northwest Territories, Canada.  
520 *Quat. Geochronol.*, **27**, 131-144, <http://dx.doi.org/10.1016/j.quageo.2015.02.001>.

521 Dibike, Y., T. Prowse, B. Bonsal, L. de Rham, and T. Saloranta, 2012: Simulation of North  
522 American lake-ice cover characteristics under contemporary and future climate conditions.  
523 *Int. J. Climatol.*, **32**, 695-709, <https://doi.org/10.1002/joc.2300>.

524 Environment and Climate Change Canada, 2020: Ice Thickness data. Accessed 18 April 2020,  
525 [https://www.canada.ca/en/environment-climate-change/services/ice-forecasts-](https://www.canada.ca/en/environment-climate-change/services/ice-forecasts-observations/latest-conditions/archive-overview/thickness-data.html)  
526 [observations/latest-conditions/archive-overview/thickness-data.html](https://www.canada.ca/en/environment-climate-change/services/ice-forecasts-observations/latest-conditions/archive-overview/thickness-data.html).

527 FLake, 2020: Useful Hints. Accessed 24 December 2020, [https://flake.igb-](https://flake.igb-berlin.de/site/download)  
528 [berlin.de/site/download](https://flake.igb-berlin.de/site/download).

529 Furgal, C., and T. Prowse, 2008: Northern Canada, In: Lemmen, D. S., F. J. Warren, J. Lacroix,  
530 E. Bush (Eds.) From impacts to adaptation: Canada in a changing climate 2007.  
531 Government of Canada, Ottawa, pp. 57-118.

532 Fyfe, J. C., and Coauthors, 2013: One hundred years of Arctic surface temperature variation  
533 due to anthropogenic influence. *Sci. Rep.*, **3**, 2645, <http://doi.org/10.1038/srep02645>.

534 Galloway, J. M., A. Macumber, R. T. Patterson, H. Falck, T. Hadlari, and E. Madsen, 2010:  
535 Paleoclimatological Assessment of the Southern Northwest Territories and Implications for  
536 the Long-Term Viability of the Tibbitt to Contwoyto Winter Road, Part I: Core Collection.  
537 Northwest Territories Geoscience Office, NWT Open Report 2010-002, 21 pp.

538 Gosling, S., G. McGregor, and J. Lowe, 2009: Climate change and heat-related mortality in six  
539 cities part 2: climate model evaluation and projected impacts from changes in the mean and

540 variability of temperature with climate change. *Int. J. Biometeorol.* **53**, 31–51,  
541 <https://doi.org/10.1007/s00484-008-0189-9>.

542 Hawkins, E., T. M. Osborne, C. Kit Ho, and A. J. Challinor, 2013: Calibration and bias  
543 correction of climate projections for crop modelling: An idealised case study over Europe.  
544 *Agr. Forest Meteorol.*, **170**, 19-31, <http://dx.doi.org/10.1016/j.agrformet.2012.04.007>.

545 Hjort, J., and Coauthors, 2018: Degrading permafrost puts Arctic infrastructure at risk by mid-  
546 century. *Nat. Commun.*, **9** (1), 5147, <https://doi.org/10.1038/s41467-018-07557-4>.

547 Ho, C. K., D. B. Stephenson, M. Collins, C. A. T. Ferro, and S. J. Brown, 2012: Calibration  
548 strategies: a source of additional uncertainty in climate change projections. *Bull. Am.*  
549 *Meteorol. Soc.*, **93**, 21-26, <https://doi.org/10.1175/2011BAMS3110.1>.

550 Hori, Y., V. Y. S. Cheng, W. A. Gough, J. Y. Jien, and L. J. S. Tsuji, 2018: Implications of  
551 projected climate change on winter road systems in Ontario's Far North, Canada. *Clim.*  
552 *Change*, **148**, 109-122, <https://doi.org/10.1007/s10584-018-2178-2>.

553 Hori, Y., W. A. Gough, K. Butler, and L. J. S. Tsuji, 2016: Trends in the seasonal length and  
554 opening dates of a winter road in the western James Bay region, Ontario, Canada. *Theor.*  
555 *Appl. Climatol.*, **129**, 1309-1320, <https://doi.org/10.1007/s00704-016-1855-1>.

556 Horton, R., and Coauthors, 2015: Contribution of changes in atmospheric circulation patterns  
557 to extreme temperature trends. *Nature*, **522**, 465-469, <https://doi.org/10.1038/nature14550>.

558 Huang, A., and Coauthors, 2019: Evaluating and improving the performance of three 1-D lake  
559 models in a large deep lake of the Central Tibetan Plateau. *JGR Atmospheres*, **124**, 3143-  
560 3167, <https://doi.org/10.1029/2018JD029610>.

561 IPCC, 2013: Summary for Policymakers. In: Climate Change 2013: The Physical Science  
562 Basis. Contribution of Working Group I to the Fifth Assessment Report of the



563 Intergovernmental Panel on Climate Change [Stocker, T.F., and Coauthors (eds.)].  
564 Cambridge University Press, Cambridge, United Kingdom and New York, NY, USA.

565 IPCC, 2018: Summary for Policymakers. In: Global Warming of 1.5°C. An IPCC Special  
566 Report on the impacts of global warming of 1.5°C above pre-industrial levels and related  
567 global greenhouse gas emission pathways, in the context of strengthening the global  
568 response to the threat of climate change, sustainable development, and efforts to eradicate  
569 poverty [Masson Delmotte, V., and Coauthors (eds.)]. In Press.

570 IPCC, 2019: Summary for Policymakers. In: IPCC Special Report on the Ocean and  
571 Cryosphere in a Changing Climate [Pörtner, H.-O., and Coauthors (eds.)]. In Press.

572 Jeffries, M. O., and K. Morris, 2006. Instantaneous daytime conductive heat flow through snow  
573 on lake ice in Alaska. *Hydrologic Process.*, **20**, 803-815,  
574 <https://doi.org/10.3402/tellusa.v64i0.17614>.

575 Jensen, O. P., B. J. Benson, J. J. Magnuson, V. M. Card, M. N. Futter, P. A. Soranno, and K.  
576 M. Stewart, 2007: Spatial analysis of ice phenology trends across the Laurentian Great  
577 Lakes region during a recent warming period. *Limnol. Oceanogr.*, **52** (5), 2013-2026,  
578 <https://doi.org/10.4319/lo.2007.52.5.2013>.

579 JVMC (Joint Venture Management Committee), 2014: Tibbitt to Contwoyto Winter Road Joint  
580 Venture. Accessed 6 Feb 2014, [www.jvtcwinterroad.ca/jvwr](http://www.jvtcwinterroad.ca/jvwr).

581 JVMC (Joint Venture Management Committee), 2015: Tibbitt to Contwoyto Winter Road Joint  
582 Venture. Accessed 24 Jan 2015, [dev.jvtcwinterroad.ca](http://dev.jvtcwinterroad.ca).

583 JVTC (Joint Venture Trucking Company), 2020: Tibbitt to Contwoyto Winter Road Joint  
584 Venture. Accessed 23 April 2020, <https://jvtcwinterroad.ca/>.

585 Kheyrollah Pour, H., C. R. Duguay, A. Martynov, and L. C. Brown, 2012: Simulation of  
586 surface temperature and ice cover of large northern lakes with 1-D models: a comparison

587 with MODIS satellite data and in situ measurements. *TELLUS A: Dynamic Meteorology*  
588 *and Climatology*, **64:1**, 17614, <https://doi.org/10.3402/tellusa.v64i0.17614>.

589 Kirillin, G., J. Hochschild, D. Mironov, A. Terzhevik, S. Golosov, and G. Nützmann, 2011:  
590 FLake-Global: Online lake model with worldwide coverage. *Environ. Modell. Softw.*, **26**,  
591 683-684, <https://doi.org/10.1016/j.envsoft.2010.12.004>.

592 Kourzeneva, E., 2014: Assimilation of lake water surface temperature observations with  
593 extended kalman filter. *Tellus A: Dynamic Meteorology and Oceanography*, **66**, 21510,  
594 <https://doi.org/10.3402/tellusa.v66.21510>.

595 Kwok, R., and Coauthors, 2009: Thinning and volume loss of the Arctic Ocean sea ice cover:  
596 2003-2008. *J. Geophys. Res.*, **114**, <https://doi.org/10.1029/2009JC005312>.

597 Lee, S., T. T. Gong, N. C. Johnson, S. B. Feldstein, and D. Pollard, 2011: On the possible link  
598 between tropical convection and the Northern Hemisphere Arctic surface air temperature  
599 change between 1958-2001. *J. Clim.*, **24**, 4350-4367,  
600 <https://doi.org/10.1175/2011JCLI4003.1>.

601 Leppäranta, M., 2010: Modelling the formation and decay of lake ice. *The impact of climate*  
602 *change on European lakes*, G. George, Ed., Springer, 63-83, [https://doi.org/10.1007/978-](https://doi.org/10.1007/978-90-481-2945-4)  
603 [90-481-2945-4](https://doi.org/10.1007/978-90-481-2945-4).

604 Melvin, A. M., and Coauthors, 2017: Climate change damages to Alaska public infrastructure  
605 and the economics of proactive adaptation. *Proc. Nat. Acad. Sci.*, **114 (2)**, E122-E131,  
606 <https://doi.org/10.1073/pnas.1611056113>.

607 Meredith, M., and Coauthors, 2019: Polar Regions. In: IPCC Special Report on the Ocean and  
608 Cryosphere in a Changing Climate Pörtner, H.-O., and Coauthors (eds.)]. In Press.

609 Mironov, D. V., 2008: Parameterization of lakes in numerical weather prediction. Description  
610 of a lake model. COSMO Technical Report, No. 11, Deutscher Wetterdienst, Offenbach  
611 am Main, Germany, 41 pp.

612 Mullan, D., and Coauthors, 2017: Climate change and the long-term viability of the world's  
613 busiest heavy haul ice road. *Theor. Appl. Climatol.*, **129**, 1089-1108,  
614 <https://doi.org/10.1007/s00704-016-1830-x>.

615 Najafi, M. R., F. W. Zwiers, and N. P. Gillett, 2015: Attribution of Arctic temperature change  
616 to greenhouse-gas and aerosol influences. *Nat. Clim. Change*, **5** (3), 246–249,  
617 <http://doi.org/10.1038/nclimate2524>.

618 Nõges, P., and Nõges, T., 2014: Weak trends in ice phenology of Estonian large lakes despite  
619 significant warming trends. *Hydrobiologia*, **731**, 5-18.

620 Overland, J. E., and Coauthors, 2015. The melting Arctic and mid-latitude weather patterns:  
621 are they connected? *J. Clim.*, **28**, 7917-7932, <https://doi.org/10.1175/JCLI-D-14-00822.1>.

622 Overland, J., and Coauthors, 2018: The urgency of Arctic change. *Polar Sci.*,  
623 <https://doi.org/10.1016/j.polar.2018.11.008>.

624 Perrin, A., and Coauthors, 2015: Economic implications of climate change adaptations for mine  
625 access roads in Northern Canada. Northern Climate ExChange, Yukon Research Centre,  
626 Yukon College, 93pp.

627 Pietikäinen, J.-P., and Coauthors, 2018: The regional climate model REMO (v2015) coupled  
628 with the 1-D freshwater lake model FLake (v1): Fenno-Scandinavian climate and lakes.  
629 *Geosci. Model Dev.*, **11**, 1321-1342, <https://doi.org/10.5194/gmd-11-1321-2018>.

630 Prowse, T. D., B. R. Bonsal, C. R. Duguay, and M. P. Lacroix, 2007: River-ice break-up/freeze-  
631 up: a review of climatic drivers, historical trends and future predictions. *Ann. Glaciol.*, **46**,  
632 443-451, <https://doi.org/10.3189/172756407782871431>.

633 Rodan, G., 2012: Storm strands truckers. Northern News Services, March 19, 2012. Accessed  
634 30 May 2020, [www.nnsl.com/preview/newspapers/stories/mar21\\_12rd.html](http://www.nnsl.com/preview/newspapers/stories/mar21_12rd.html).

635 Rontu, L., K. Eerola, and M. Horttanainen, 2019: Validation of lake surface state in the  
636 HIRLAM v.7.4 numerical weather prediction model against in situ measurements in  
637 Finland. *Geosci. Model Dev.*, **12**, 3707-3723, <https://doi.org/10.5194/gmd-12-3707-2019>.

638 Shabbar, A., M. Khandekar, 1996: The impact of El Niño-Southern Oscillation on the  
639 temperature field over Canada. *Atmos. Ocean*, **34**, 401-416,  
640 <https://doi.org/10.1080/07055900.1996.9649570>.

641 Sim, T. G., G. T. Swindles, P. J. Morris, M. Gałka, D. Mullan, and J. M. Galloway, 2019:  
642 Pathways for ecological change in Canadian High Arctic wetlands under rapid twentieth  
643 century warming. *Geophys. Res. Lett.*, **46**, 4726–4737,  
644 <https://doi.org/10.1029/2019GL082611>.

645 Sladen, W. E., S. A. Wolfe, and P. D. Morse, 2020: Evaluation of threshold freezing conditions  
646 for winter road construction over discontinuous permafrost peatlands, subarctic Canada.  
647 *Cold Reg. Sci. Technol.*, **170**, 102930, <https://doi.org/10.1016/j.coldregions.2019.102930>.

648 Swindles, G. T., and Coauthors, 2015: The long-term fate of permafrost peatlands under rapid  
649 climate warming. *Sci. Rep.*, **5**, 17951, <https://doi.org/10.1038/srep17951>.

650 Taylor, K. E., R. J. Stouffer, and G. A. Meehl, 2012: An overview of CMIP5 and the  
651 experiment design. *Bull. Amer. Meteor. Soc.*, **93**, 485-498. [https://doi.org/10.1175/BAMS-](https://doi.org/10.1175/BAMS-D-11-00094.1)  
652 [D-11-00094.1](https://doi.org/10.1175/BAMS-D-11-00094.1).

653 Timmermann, A., and Coauthors, 2018: El Niño–Southern Oscillation complexity. *Nature*,  
654 **559**, 535-545, <https://doi.org/10.1038/s41586-018-0252-6>.

655 UNFCCC, 2015: Paris Agreement. Accessed 26 June 2020,  
656 [https://unfccc.int/files/essential\\_background/convention/application/pdf/english\\_paris\\_ag](https://unfccc.int/files/essential_background/convention/application/pdf/english_paris_agreement.pdf)  
657 [reement.pdf](https://unfccc.int/files/essential_background/convention/application/pdf/english_paris_agreement.pdf).

658 van Vuuren, D. P., and Coauthors, 2011: The representative concentration pathways: an  
659 overview. *Clim. Change*, **109**, 5-31, <https://doi.org/10.1007/s10584-011-0148-z>.

660 Wallace, J. M., and D. S. Gutzler, 1981: Teleconnections in the Geopotential Height Field  
661 during the Northern Hemisphere Winter. *Mon. Wea. Rev.*, **109** (4), 784-812,  
662 [https://doi.org/10.1175/1520-0493\(1981\)109<0784:TITGHF>2.0.CO;2](https://doi.org/10.1175/1520-0493(1981)109<0784:TITGHF>2.0.CO;2).

663 Weedon, G. P., G. Balsamo, N. Bellouin, S. Gomes, M. J. Best, and P. Viterbo, 2014: The  
664 WFDEI meteorological forcing data set: WATCH Forcing Data methodology applied to  
665 ERA- Interim reanalysis data. *Water Resour. Res.*, **50**, 7505-7514,  
666 <https://doi.org/10.1002/2014WR015638>.

667 Yang, W., and G. Magnusdottir, 2018: Year-to-year variability in Arctic minimum sea ice  
668 extent and its preconditions in observations and the CESM large ensemble simulations. *Sci.*  
669 *Rep.*, <https://doi.org/10.1038/s41598-018-27149-y>.

670 Yang, Y., B. Cheng, E. Kourzeneva, T. Semmler, L. Rontu, M. Leppäranta, K. Shirasawa, and  
671 Z. J. Li, 2013: Modelling experiments on air-snow-ice interactions over Kilpisjärvi, a lake  
672 in northern Finland. *Boreal Environ. Res.*, **18**, 341-358.

673

674

675

676

677

678

679 **Appendix Tables**

680

Model Ensemble	RMSE	1.5°C	2°C	4°C
IPSL-CM5A-LR r1i1p1	1.16	2033-2053	2039-2059	2074-2094
ICHEC EC-Earth r2i1p1	1.42	2029-2049	2047-2067	
NOAA GFDL-ESM2G r1i1p1	1.52	2037-2057	2058-2078	
CSIRO-QCCCE CSIRO-Mk3-6-0 r9i1p1	1.54	2031-2051	2043-2063	
IPSL-CM5A-LR r4i1p1	1.37	2027-2047		
CSIRO-QCCCE CSIRO-Mk3-6-0 r8i1p1	1.46		2048-2068	
IPSL-CM5A-LR r3i1p1	1.78			2075-2095
MIROC5 r2i1p1	1.82			2066-2086
MIROC5 r3i1p1	1.90			2069-2089
CSIRO-QCCCE CSIRO-Mk-3-6-0 r1i1p1	1.92			2079-2099

681

682 **Table A1.** All 15 shortlisted scenarios as used for FLake modelling. Root Mean Square Error  
 683 (RMSE) is provided, along with the extracted years for each scenario. Twenty-year time  
 684 periods were taken from 1 October on the start year to 30 September on the end year to conform  
 685 to the temporal basis of FLake modelling and represent the 20-year mean period when  
 686 temperatures first exceed the RMTI associated with each of the three GMTIs.

687

688

689

690

691

692

Year	Open Date	Close Date	Duration (Days)	No. Loads	Tonnes
2001	1 Feb	13 Apr	72	7,981	245,586
2002	26 Jan	16 Apr	81	7,735	256,915
2003	1 Feb	2 Apr	61	5,243	198,818
2004	28 Jan	31 Mar	63	5,091	179,144
2005	26 Jan	5 Apr	70	7,607	252,533
2006	4 Feb	26 Mar	50	6,841	177,674
2007	27 Jan	9 Apr	73	10,922	330,002
2008	29 Jan	7 Apr	62	7,484	245,585
2009	1 Feb	25 Mar	50	5,377	173,195
2010	4 Feb	24 Mar	46	3,508	120,020
2011	28 Jan	31 Mar	63	6,832	239,000
2012	1 Feb	28 Mar	59	6,551	210,188
2013	30 Jan	31 Mar	61	6,017	223,206
2014	30 Jan	1 Apr	62	7,069	243,928
2015	30 Jan	31 Mar	61	8,915	305,215
2016	9 Feb	24 Mar	44	8,766	262,261
2017	1 Feb	29 Mar	57	8,241	279,484
2018	1 Feb	31 Mar	61	8,209	303,725
2019	1 Feb	31 Mar	59	7,489	257,176
2020	31 Jan	8 Apr	68	7,072	230,497

693

694 **Table A2.** Historical Operational Season Statistics for the TCWR (JVTC, 2020).

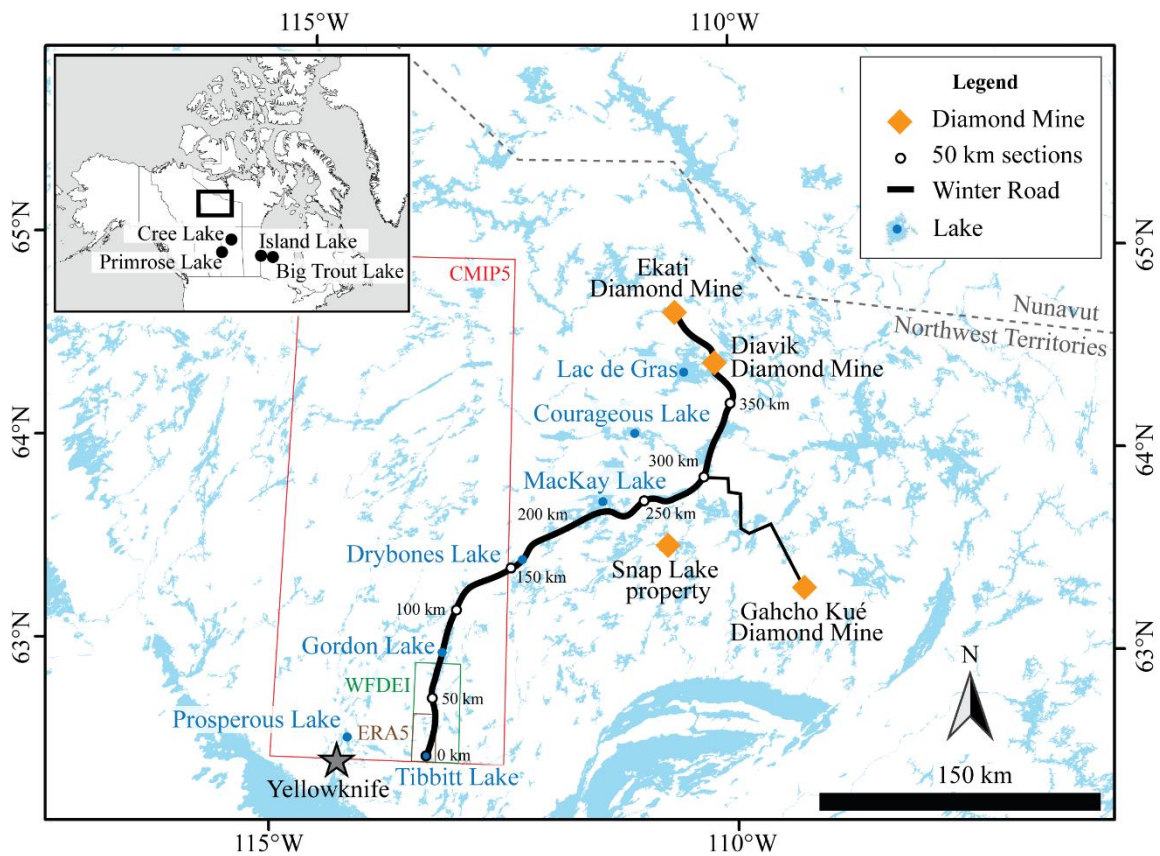
695

696

697 **Figures**

698

699



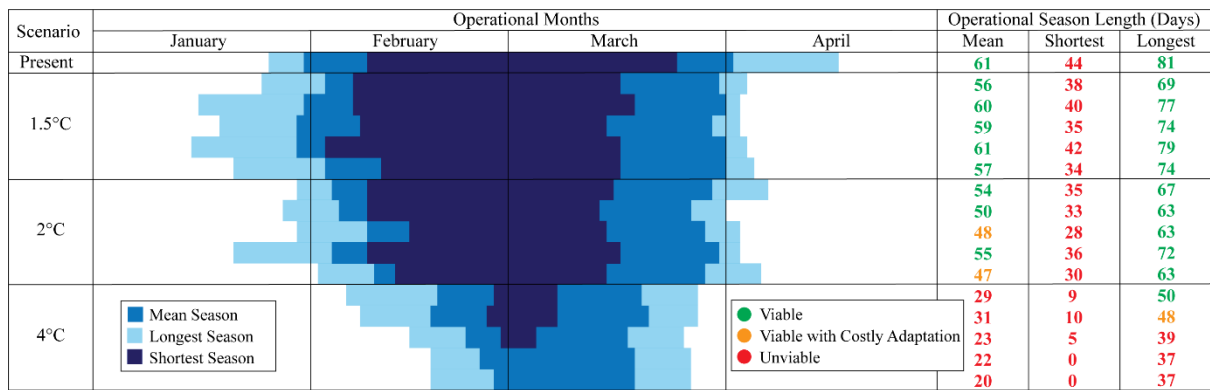
700

701 **Figure 1.** The TCWR study region. The three transparent boxes show the spatial resolution of  
702 the ERA5 (0.25° x 0.25°) and WFDEI (0.5° x 0.5°) climate observations, as well as the CMIP5  
703 climate model scenarios (*ca.* 2.5° x 2.5° but variable from model to model). The locations of  
704 the four lakes used for model validation are also shown in the inset map.

705

706





707

708

709

710

711

712

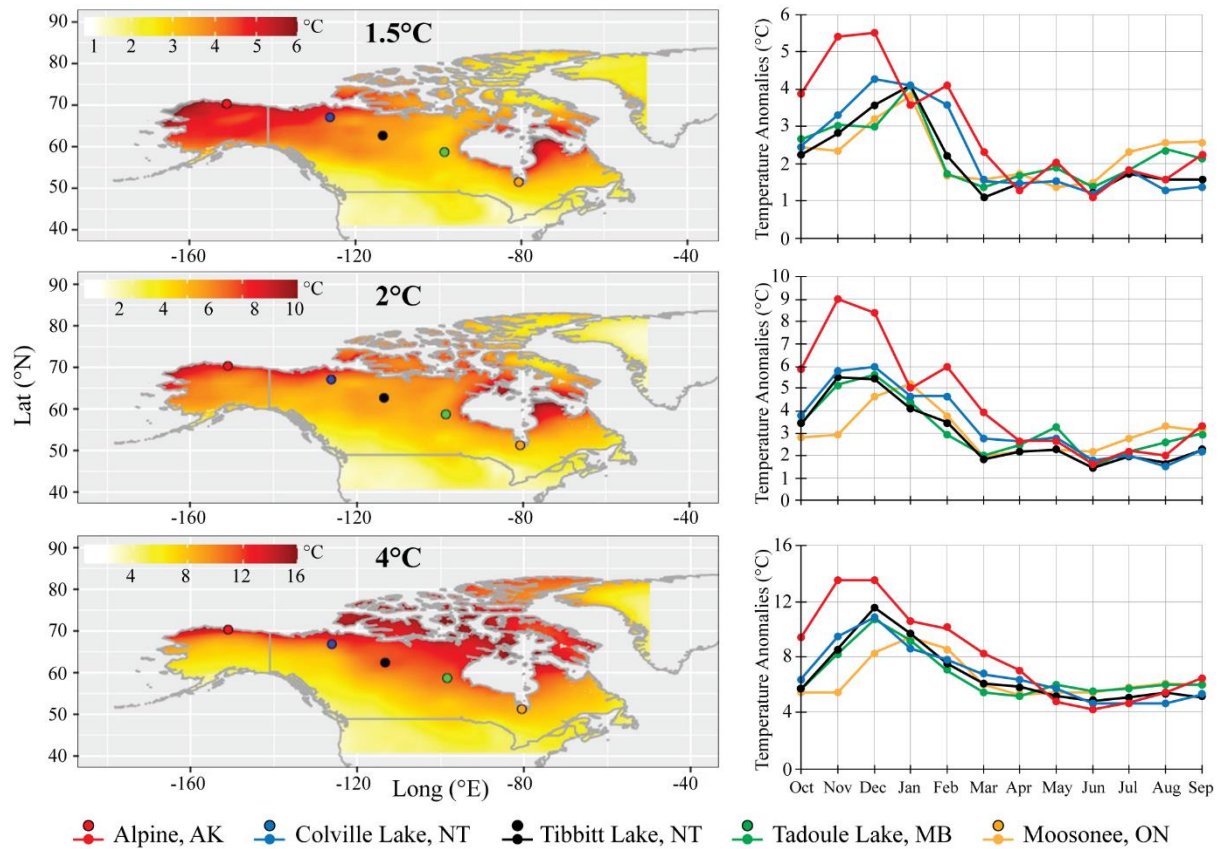
713

714

715

716

**Figure 2.** TCWR operational season as observed for the present (mean of 2001-2020 observations taken from JVTC (2020)) (n=1) and simulated by FLake for the future under 15 climate scenarios corresponding to a GMTI of 1.5°C (n=5), 2°C (n=5) and 4°C (n=5). The mean of the 20-year observations / simulations is shown in medium blue, while the year with the shortest (longest) season is shown in dark (light) blue. Also shown is the operational season length (days) for the mean, shortest and longest years in a traffic light colour system following the scenarios outlined in Perrin et al. (2015):  $\geq 50$  days = green (viable); 45-49 days = amber (viable with costly adaptation);  $< 45$  days = red (unviable).



717

718

719

720

721

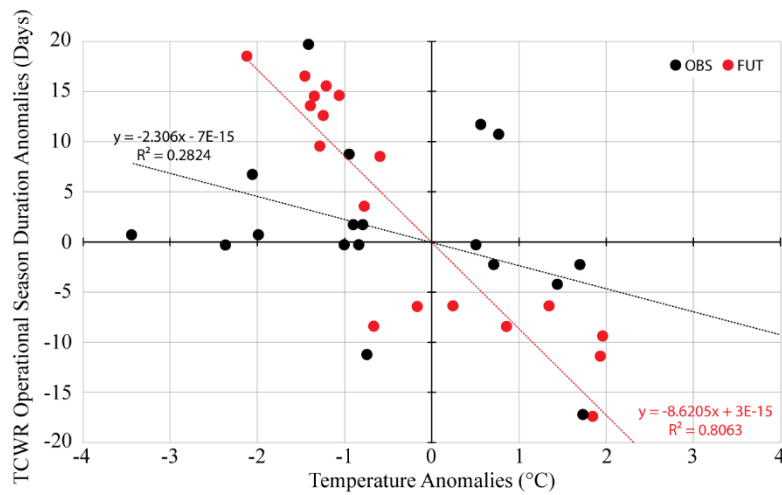
722

723

724

725

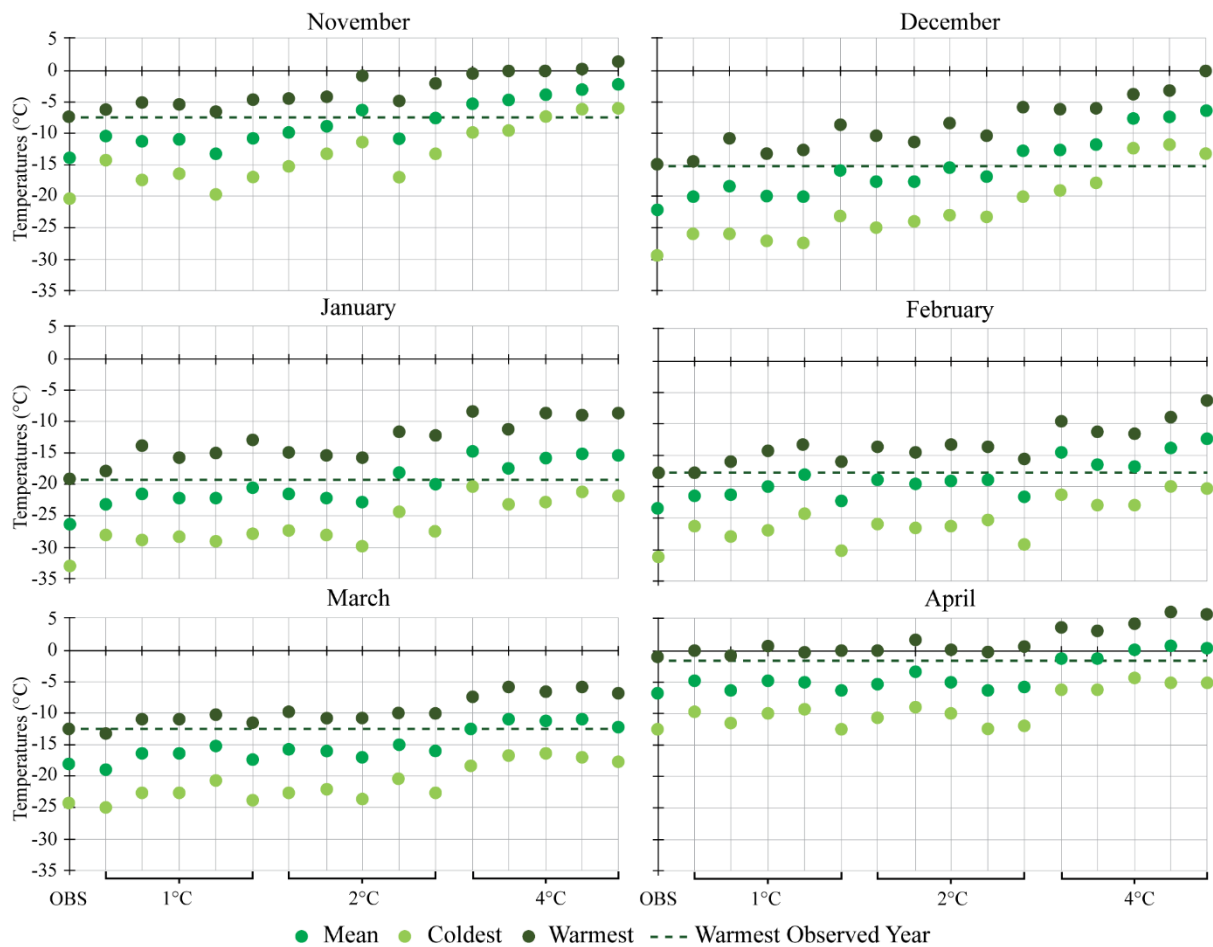
**Figure 3.** Map panels: mean projected December temperature anomalies for the northern half of North America. Temperature anomalies are expressed as the mean of the models analysed in this study at a GMTI of 1.5°C, 2°C and 4°C from the mean 1986-2005 observed period. Graph panels: Temperature anomalies (calculated in the same way as above) for each month of the year for five winter roads in North America (including the TCWR, as represented by Tibbitt Lake, NT). Two-letter state/province/territory codes are used for the five winter road locations – AK: Alaska; MB: Manitoba; NT: Northwest Territories; ON: Ontario.



726

727 **Figure 4. November-April mean** temperature (°C) and TCWR seasonal duration (days)  
 728 anomalies for the Tibbit Lake region of the TCWR. Anomalies for each year of the 20-year  
 729 observed record / model simulations are expressed as changes relative to the mean of that same  
 730 20-year period. Black points represent observations (OBS) for 2000-2020 and red points  
 731 represent the most extreme model simulation (FUT) under a 4°C GMTI – in this case for 2079-  
 732 2099 – the 20-year period when temperatures first rise the RMTI equivalent of 4°C GMTI  
 733 above preindustrial temperatures.

734



735

736 **Figure 5.** November-April temperatures at Tibbitt Lake as observed (OBS) for the present

737 (n=1) and simulated for the future under 15 climate scenarios corresponding to a GMTI of

738 1.5°C (n=5), 2°C (n=5) and 4°C (n=5). The mean of the 20-year observations / simulations is

739 shown in medium green, while the year with the coldest (warmest) temperatures for each

740 particular month is shown in light (dark) green. The dashed line represents observed

741 temperatures during the warmest year (mean of November-April).

742

743

744

745

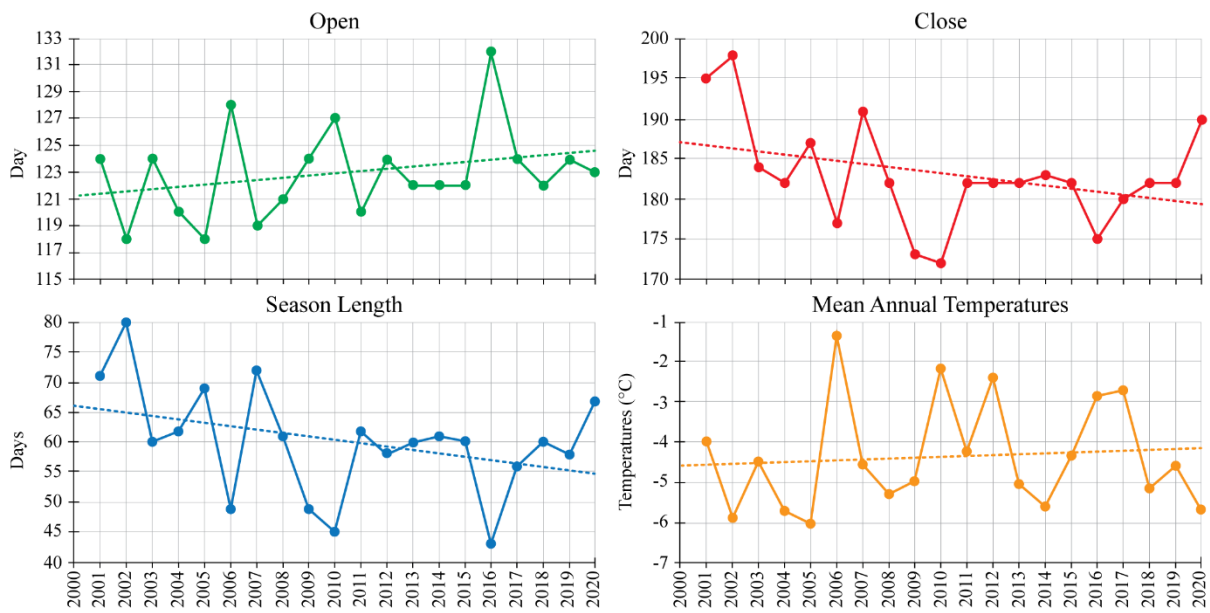
746

747

748 **Appendix Figures**

749

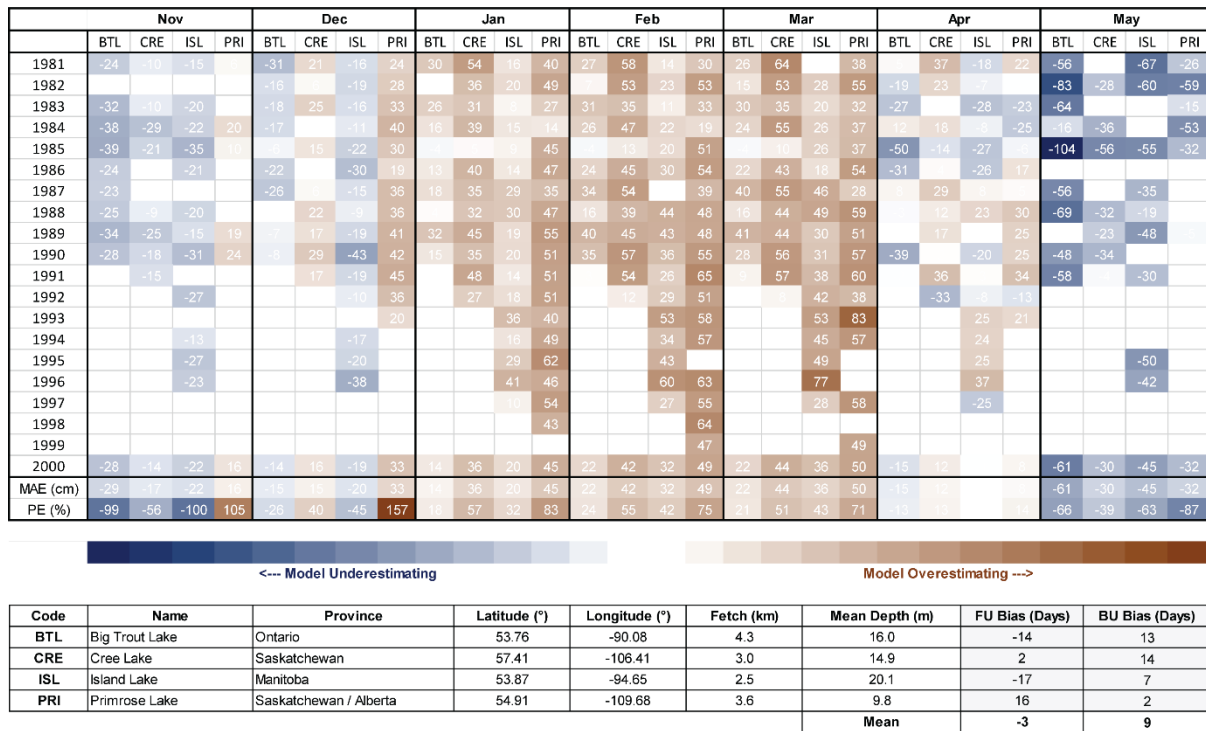
750



751

752 **Figure A1.** Changes in the TCWR open date (top left) and close date (top right) from 2001-  
 753 2020 (JVTC, 2020) and mean annual air temperatures for Tibbitt Lake from 2001-2020. For  
 754 the top panels and the bottom left panel, dates are expressed as days since the start of the  
 755 hydrological year on 1 October. Mean annual air temperatures are calculated for hydrological  
 756 years, starting on 1 October and ending on 30 September the next year.

757



759

760

761

762

763

764

765

766

767

768

769

770

771

772

**Figure A2.** Absolute error (observed ice thickness minus modelled ice thickness) for four analogous shallow sub-arctic Canadian lakes (the details of which are provided in the table part of the figure) covering a minimum of ten years during the period 1981-2000. Results are provided on a monthly basis, with mean absolute error (MAE) calculated for all years with measurements and percentage error (PE) calculated as relative error multiplied by 100. Also provided in the table part of the figure is freezeup (FU) bias and breakup (BU) bias – calculated as observed FU/BU minus FLake simulated FU/BU for each lake across the same years as the data used to calculate absolute error in the main part of the figure. Negative (positive) numbers indicate FU/BU is simulated later (earlier) than observed.